Journal of Magnetic Resonance 322 (2021) 106877

Contents lists available at ScienceDirect

Journal of Magnetic Resonance

journal homepage: www.elsevier.com/locate/jmr

Metamaterial inspired wireless coil for clinical breast imaging

Viktor Puchnin [a], Georgiy Solomakha [a], Anton Nikulin [b], Arthur W. Magill [c], Anna Andreychenko [a,d], Alena Shchelokova [a,*]

[a] Department of Physics and Engineering, ITMO University, Saint Petersburg, Russia
[b] Institut Langevin, ESPCI Paris, CNRS, PSL University, Paris, France
[c] Medical Physics in Radiology, German Cancer Research Center (DKFZ), Heidelberg, Germany
[d] Research and Practical Clinical Center for Diagnostics and Telemedicine Technologies of the Moscow Health Care Department, Moscow, Russia

ARTICLE INFO

Article history:
Received 13 July 2020
Revised 17 November 2020
Accepted 18 November 2020
Available online 21 November 2020

Keywords:
Metamaterial inspired RF coils
Split-loop resonator
Wireless coil
Breast MRI
SNR enhancement
Transmit efficiency
Specific absorption rate

ABSTRACT

In this work, we propose an application of a metamaterial inspired volumetric wireless coil (WLC) based on coupled split-loop resonators for targeted breast MRI at 1.5 T. Due to strong electromagnetic coupling with the body coil, the metamaterial inspired WLC locally focuses radiofrequency (RF) magnetic flux in the target region, thus improving both transmit and receive performance of the external body coil. This leads to substantial enhancement in local transmit efficiency and improvement of RF safety. Phantom images showed a tenfold increase of signal-to-noise ratio (SNR) in the region-of-interest (ROI) and, at the same time, an almost 50-fold reduction in transmit power relative to the same body coil used alone.

1. Introduction

Breast cancer is the most common cancer among women, worldwide [1,2]. Increased availability of high-quality diagnosis, preventative, and treatment methods could potentially reduce female breast cancer mortality [1]. MRI has the highest sensitivity to breast cancer, relative to other non-invasive imaging techniques such as ultrasound or mammography. This is especially relevant for young women with dense breast tissue [3,4] or with breast implants [5], when mammography is often not capable of distinguishing between healthy and cancerous tissues. Thus, use of MRI is increasingly essential in the detection of breast cancer in daily practice [6]. However, due to associated high costs and lengthy procedures, MR-screening is not widely applied. At the same time, the feasibility of breast cancer screening with MRI is being investigated (e.g., shortening of the protocols [7]). To produce proper quality breast images, i.e., with high SNR, it is necessary to use a specialized breast RF receive-coil. Such a coil is not standard equipment of an MR scanner and has to be purchased separately. Because of the associated extra costs, a dedicated breast coil is often not available at clinical MR scanners, and a body receive-array is used instead, compromising the SNR of breast images. Finally, the diagnostic quality of the acquired MR images can be hampered due to patient discomfort caused by the necessity to lay still for more than half an hour. As a result, despite its potential superiority as a medical imaging modality, MRI is not used for extensive population screening and is advised only for those women with the highest risks to develop breast cancer.

A recently proposed targeted MRI concept demonstrated novel opportunities for high-quality, specialized studies of the breast within clinical 3 T MRI [8]. The concept is based on passive focusing of the RF magnetic field of the body coil to maximize its efficiency for small areas with the aid of an artificial resonator made of ceramic. In a prospective study, it was shown that 1.5 T breast MRI has comparable diagnostic accuracy to a 3 T MRI despite a larger associated sensitivity of the latter [9]. Given the much higher prevalence of 1.5 T MR scanners over 3 T, breast MRI at 1.5 T is more suitable for screening purposes than 3 T. Thus, there is a need for a targeted MRI concept for breast imaging at 1.5 T as well. However, the application of dielectric materials and resonators is limited for lower fields (e.g.,1.5 T) since extremely high relative permittivity values of thousands are required [10]. Alternatively, artificial resonators made of metamaterial inspired structures can boost locally transmit efficiency and receive sensitivity of a body

* Corresponding author at: Department of Physics and Engineering, ITMO University, Kronverkskiy Prospekt, 49A, Saint Petersburg 197101, Russia.
E-mail address: a.schelokova@metalab.ifmo.ru (A. Shchelokova).

https://doi.org/10.1016/j.jmr.2020.106877
1090-7807/

coil, improving RF safety [11] and SNR [12,13]. The main advantages of such resonators are simplicity of the design (hence, robustness and ease of maintenance), absence of RF cables, and as a consequence, low cost. Moreover, these devices can be directly integrated and applied within any clinical MR scanner with no modifications to the scanner hardware.

In this study we demonstrate, via electromagnetic simulations and phantom experiments, a metamaterial inspired volumetric WLC, a "metasolenoid" [14], for breast imaging at 1.5 T. The structure consists of periodically arranged inductively coupled split-loop resonators (SLRs) made of telescopic brass tubes loaded at their ends with capacitors implemented as copper strips on two printed circuit boards (PCBs). Focusing the RF magnetic field inside the ROI with the proposed "metasolenoid" allows substantial improvement of SNR and a reduction of input power compared to a conventional body coil used alone. This WLC was first proposed and as a proof of the concept applied for the wrist imaging in [13]. Here, the metamaterial inspired WLC design is optimized for the breast, i.e., the WLC is placed directly near the body and asymmetrically relative to the body coil isocenter. That leads to the different coupling of the resonance structure with the external source-coil compared to when the WLC is located directly in the center [13]. Thus, we performed a detailed study of the behavior and influence of the metamaterial-inspired WLC on the main MRI characteristics: transmit efficiency, SNR, RF safety. Moreover, via numerical simulations with different sizes of voxel models, we evaluated the possibility and effectiveness of using the WLC for women with different body mass indexes.

2. Methods

2.1. WLC design

The design of the metamaterial-inspired volumetric WLC is depicted in Fig. 1(a). To cover an average breast volume 320 ml [15] we assume the suitable dimensions of the resonator are no less than $100 \times 100 \times 100$ mm^3. The WLC consists of rectangular electromagnetically coupled SLRs. Every split loop resonator contains two parallel telescopic brass tubes connected at the ends by two PCB capacitors implemented as overlapping copper strips printed on the opposite sides of the dielectric substrate. Each telescopic tube is constructed from two coaxial tubes of a slightly different radii (1.0 mm and 1.5 mm) sliding over one another.

The proposed structure supports a set of volumetric eigenmodes [16]. In this study, we use a fundamental mode, which has a homogeneous magnetic field distribution inside the coil volume [17], while the electric field is mostly concentrated inside the PCB capacitors. Capacitance and the length of the tubes are adjusted to tune the fundamental mode to the proton Larmor frequency of 63.68 MHz at 1.5 T [Fig. 1(b)] while keeping the resonator size suitable to perform breast imaging. Also worth noting, that the resonance frequency of the structure eigenmode may be fine-tuned by adjusting the length of the telescopic tubes [Fig. 1(c)] that changes the inductance of SLRs.

Since the choice of dielectric substrates for production is limited, the dimensions of metal capacitors (for tuning to a working frequency) and their quantity are subsequently restricted. We choose the PCBs made from Arlon 255C (Rogers Corp., Chandler, AZ, USA) with $\varepsilon = 2.5$ and $\tan\delta = 0.0013$ at 10 GHz and dimensions $164 \times 114 \times 1$ mm^3. Thus, the width and length of the internal PCB capacitors are 9×69 mm^2 respectively, and the outer strips are 9×160 mm^2. As a result, together with the gaps, we could fit ten strips on the PCB, i.e., the WLC consists of ten split loops, maintaining compactness and ease of manufacture.

2.2. Electromagnetic simulations

All electromagnetic simulations were performed in CST Studio Suite 2017 (CST AG, Darmstadt, Germany) using the Finite Integral Technique time domain solver. To evaluate the operational frequency of the WLC, we added a small non-resonant loop-antenna placed above the "metasolenoid" [see Fig. 1(a)].

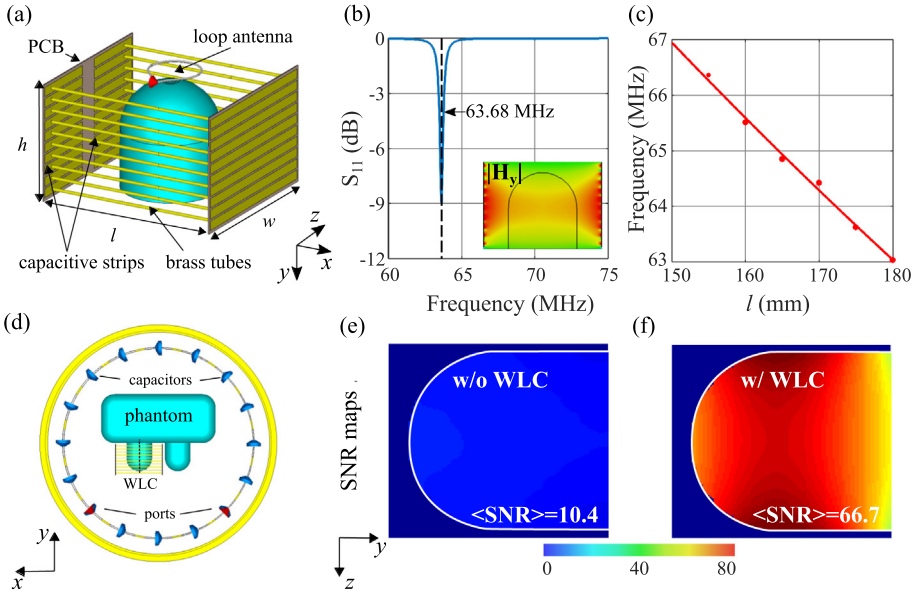

Fig. 1. (a) Schematic view of the metamaterial inspired WLC together with a breast phantom and a small loop-antenna. The coil is assembled from ten identical split-loop resonators (SLRs) consisting of parallel telescopic brass tubes of the length ℓ and two standard dual-layer printed-circuit boards (PCBs) with capacitive strips. The PCBs have dimensions: h = 114 mm, w = 164 mm, thickness = 1 mm. (b) Reflection coefficient (S_{11}) of the loop antenna placed above the WLC with ℓ = 176 mm. The dashed line indicates the Larmor frequency of 63.68 MHz. (c) The resonance frequency of the fundamental eigenmode as a function of the tube length (ℓ). (d) Schematic view of the model used in the numerical study: birdcage coil together with body and breast phantoms and the metamaterial inspired structure placed around one of the breast phantoms. Signal-to-noise ratio (SNR) maps for the birdcage coil alone (e) and with the WLC (f) for the central plane across the breast indicated with a black dashed line in panel (d). The white line indicates the contour of the breast phantom.

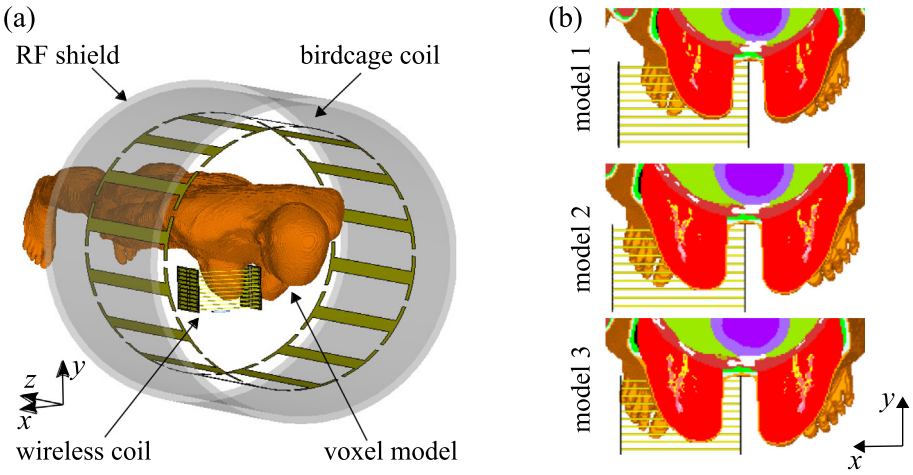

Fig. 2. (a) General view of the numerical setup: voxel model placed inside the birdcage coil with WLC. (b) The view of different size voxel models with respect to the WLC volume (central XY plane): model 1 corresponds to 70% of the initial (average) model 2, model 3 corresponds to 120% of model 2.

To evaluate the impact of the metamaterial inspired WLC on the SNR, we first simulated a body-sized birdcage coil loaded with a simple geometric phantom, without and with the WLC placed around one of the breasts [Fig. 1(d)]. The phantom consisted of two homogeneous regions to represent the breasts (hemispheres of 100 mm diameter connected to 100 mm high cylinders, $\varepsilon = 78, \sigma = 0.19$ S/m) attached to a homogeneous rectangular box ($600 \times 420 \times 180$ mm^3 with a 50 mm fillet applied to all edges, $\varepsilon = 78, \sigma = 0.45$ S/m). The birdcage coil was a high-pass cylindrical quadrature coil with 16 legs, tuned, and matched at 63.68 MHz. A circularly polarized RF magnetic field (B_1) was created by two feeding ports with 90° phase difference. When one of the B_1 components of the birdcage coil is normal to the plane of the SLRs of the 'metasolenoid', the latter inductively couples with the external source coil and focuses the magnetic flux within its cavity. We estimate the SNR as the ratio of the $|B_1^-|$-field in the ROI divided to the square root of power dissipated within the phantoms.

Simulations then were repeated using realistic female body models in place of the geometric homogeneous phantom. The body model was based on Ella from the Virtual Family [18]. Because the Ella model was derived from MRI scans of a woman in the supine position, we modified it to add breast phantom No. 1 from the UWCEM Numerical Breast Phantom Repository[1] [21]. This was done using the method described by Rispoli et al. [19] and provided source code[2], modified to import the model into CST. The breast model includes five tissues representing a mixture of adipose and fibroglandular tissue, in volume ratios 0/100%, 25/75%, 50/50%, 75/25%, and 100/0%, and skin. The fusion was done using a 0.5 mm isotropic mesh followed by resampling to 2 mm. The whole body model was then rescaled by ±10% on each axis to generate three models of different sizes [Fig. 2(b)]: (1) a small model with a total weight of 43.4 kg; (2) the initial voxel model with a total weight of 59.4 kg; (3) a large model with a total weight of 72.8 kg. The birdcage coil was matched in the presence of each model, and the WLC was tuned to 63.68 MHz by changing the length of brass tubes. B_1^+ fields and 10 g-averaged SAR were then calculated without and with the WLC present.

WLC' performance was evaluated by comparing transmit and SAR efficiencies, defined as the root mean squared value (RMS) $|B_1^+|_{\mathrm{RMS}}$ in the ROI per 1 W of accepted power, and $|B_1^+|_{\mathrm{RMS}}$ in the ROI per square root of maximum local SAR ($\mathrm{maxSAR}_{\mathrm{av.10g}}$), respectively. Transmit, and SAR efficiency gains were then defined as the ratio of these values with and without the WLC present.

2.3. Experimental studies

The prototype of the metamaterial inspired WLC was built by arranging two periodic sets of ten parallel telescopic tubes soldered at their ends to solder-covered copper strips on two PCBs forming structural capacity. The structure has the same dimensions as used in numerical studies. Fig. 4(a) shows the manufactured WLC with the homogeneous breast phantom placed inside. The phantom shell was 3D printed (Pro2, Raise3D, Rotterdam, Netherlands) in polylactic acid (PLA) with a height of 100 mm and a base radius of 50 mm. The phantom solution consisted of distilled water, NaCl (0.75 g/l), agarose ($C_{12}H_{18}O_9$, 10 g/l) and a gadolinium-based MRI contrast agent (0.5 ml/l) to reduce spin–lattice relaxation time T_1. The phantom permittivity and conductivity were measured to be $\varepsilon = 78$ and $\sigma = 0.19$ S/m at 63.68 MHz using a coaxial probe (DAK-12, SPEAG, Zurich, Switzerland) placed on top of a phantom material and a vector network analyzer (ZVA 20, Rohde & Schwarz, Munich, Germany).

MRI experiments were performed on a 1.5 T clinical MRI scanner (MAGNETOM Espree, Siemens, Erlangen, Germany) at Federal Almazov North-West Medical Research Centre (Saint Petersburg, Russia). We also used a large distilled water with NaCl and $MnCl_2 \times 4H_2O$ phantom that mimicked a body (Siemens loaded body phantom) shown in Fig. 4(b). First, the longitudinal relaxation time T_1 = 288 ms of the created breast phantom was estimated using inversion-recovery measurements: STIR sequence, flip angle = 150°, TR/TE = 4000/10 ms, field of view = 107×126 mm^2, acquisition matrix = 256×153, TI is varied 25–400 ms.

MR images of the breast phantom were acquired using a gradient echo sequence: flip angle = 40°, TR/TE = 2000/4.8 ms, field of view = 129×143 mm^2, acquisition matrix = 128×116, slice thickness 3 mm. We used the body birdcage coil both for transmission and reception without and with WLC present. To estimate the impact of the WLC tuning on its efficiency (SNR gain and RF pulse amplitude enhancement), we acquire a set of images changing the tube length (i.e., the WLC eigenmode resonant frequency). The transmit RF power level of the scanner was calibrated to ensure the actual flip angle in the ROI equal to the nominal flip angle set by an operator.

The SNR gain was calculated by analyzing images obtained without and with the WLC using MATLAB R2016b (The Mathworks,

[1] http://uwcem.ece.wisc.edu/phantomRepository.html.
[2] https://github.com/rispoli-lab/Bilateral-Breast-Fusion-.

Natick, MA, USA). The SNR of each image was calculated by dividing a mean value of the signal from the breast phantom by the standard deviation of noise in an image acquired with no RF excitation.

3. Results

3.1. Electromagnetic simulations

Fig. 1(e), (f) shows simulated SNR maps in the central slice of the breast phantom for the body-sized birdcage coil without and with the WLC, respectively. The mean SNR across the central plane of the breast phantom increased 6.4-fold in the presence of WLC. The $|B_1^+|$ distribution inside the breast phantom is similar to the magnetic field ($|H_y|$) distribution for WLC fundamental eigenmode [inset in Fig. 1(b)]. When the body coil was used alone, $|B_1^+| = 0.20 \pm 0.01\mu T$ (mean ± std), which increased to $|B_1^+| = 1.23 \pm 0.15\mu T$ in presence of the WLC.

Fig. 3 demonstrates simulated $|B_1^+|_{RMS}$ and $SAR_{av.10\ g}$ maps for the average size voxel model (model 2) inside the body coil without and with the proposed WLC placed around one of the breasts. Strong localization of the B_1^+ field in the breast region in the presence of the WLC leads to a 5.9-fold enhancement in transmit efficiency [compare Fig. 3(a) and (b)]. At the same time, the maximum local $SAR_{av.10\ g}$ in the body model is increased red 2.3 times when the WLC is added [Fig. 3(d,e)]. The local $SAR_{av.10\ g}$ maximum in the body model (depicted as a white circle in Fig. 3(d-f)] is located in the muscles of the back with the birdcage coil only, and in the pectoral muscles for the case with the WLC. To maintain an RMS $|B_1^+|$ of 0.29 μT in the ROI, the transmit power should be reduced from 1 W to 30 mW when the WLC is added, reducing the maximum local $SAR_{av.10\ g}$ by a factor of 18.

Table 1 summarizes the electromagnetic simulation results for all three female voxel models, without and with the WLC present. When using the body coil alone, the highest transmit efficiency was seen for the smallest body model (model 1), which is reasonable as the quality factor of the body coil is higher in the presence of a smaller load. The highest maximum local $SAR_{av.10g}$ was also seen for this model. SAR efficiency was found to vary little across all body models (∓13%). In the presence of the WLC, interaction between the electromagnetic fields and the body is more complicated. The WLC redistributes electromagnetic field, localizing the magnetic field within its cavity, while electric field is almost entirely confined between the capacitive copper strips, i.e close to the body (see electric field maps in Supplementary Fig. 1). As was mentioned above, the quality factor of the body coil is higher in the presence of a smaller load; the same is for the WLC. However, in the case of model 1, strong coupling between two resonators occurs, and more power is reflected compared to model 2. Thus, transmit efficiency for model 2 is equal to 1.67 $\mu T/\sqrt{W}$ that is 4% higher than for model 1. With a further increase in body volume, a decrease in the quality factor is more strongly affected, and thus the RF magnetic field in the breast becomes lower: 1.06 $\mu T/\sqrt{W}$ for model 3. A decreasing of the electric field due to a change in the quality factor affects the change in SAR, so we

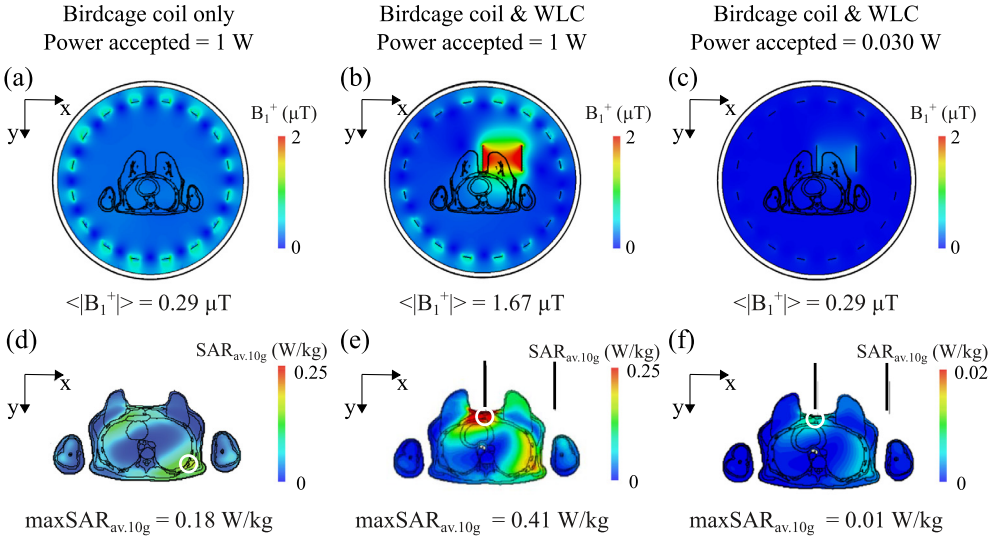

Fig. 3. Numerically calculated $|B_1^+|_{RMS}$ maps (a–c) and $SAR_{av.10\ g}$ maps (d–f) for the average sized voxel model (No. 2) placed inside the birdcage coil without and with the WLC, respectively. The $|B_1^+|_{RMS}$ value was calculated only for the volume of the resonator in the breast area (ROI). (d-f) $SAR_{av.10\ g}$ distributions are build up through the local maximum plane. Local $SAR_{av.10\ g}$ maxima are indicated with white circles. Panel (f) was re-scaled to better visualize the SAR distribution.

Table 1
Numerically calculated results of transmit and SAR efficiencies without and with the WLC for different voxel models.

	WLC	Model 1	Model 2	Model 3	Units
$\|B_1^+\|/\sqrt{P_{acc}}$	no	0.33	0.29	0.26	$\left[\mu T/\sqrt{W}\right]$
	yes	1.61	1.67	1.06	
$maxSAR_{av.10g}$	no	0.19	0.18	0.16	[W/kg]
	yes	0.48	0.41	0.27	
$\|B_1^+\|/\sqrt{maxSAR_{av.10g}}$	no	1.08	0.95	0.91	$\left[\mu T/\sqrt{W/kg}\right]$
	yes	3.28	3.67	2.89	
Transmit efficiency gain	n/a	4.9	5.8	4.2	times
SAR efficiency gain	n/a	3.1	3.9	3.2	times

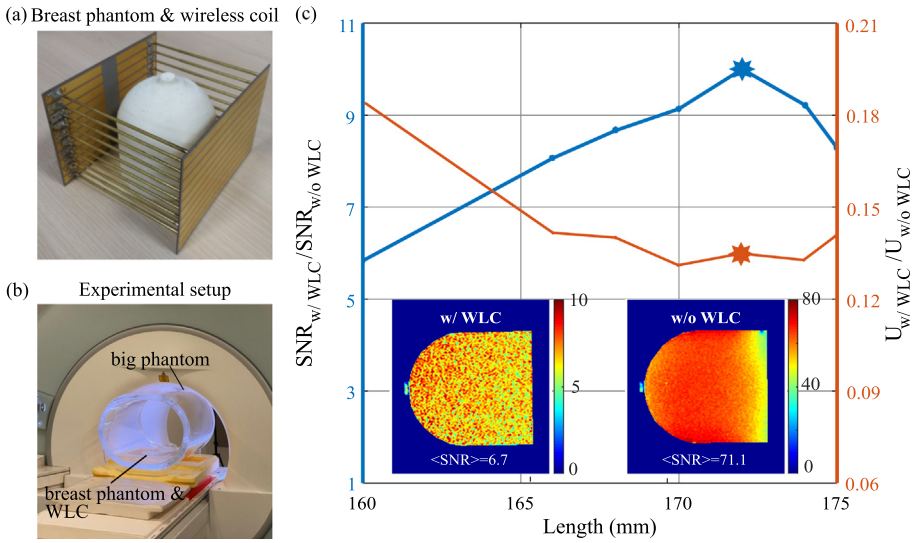

Fig. 4. Photographs of the (a) WLC prototype together with breast phantom, and (b) experimental setup including body-sized birdcage coil, body phantom, breast phantom, and WLC; (c) SNR gain (blue) and reduction in required transmit voltage (red) as a function of tubes length. Insets in (c) show SNR maps without the WLC, and with the WLC set to the optimum length ℓ = 172 mm (note the different colour scales), this case is indicated with stars on the curves. (For interpretation of the references to colour in this figure legend, the reader is referred to the web version of this article.)

observed the highest $SAR_{av.10g}$ = 0.48 W/kg for the smallest load. As a result, transmit efficiency gains in the presence of the WLC are 4.9, 5.8, and 4.2-fold for models 1, 2, and 3, respectively, whereas SAR efficiency gains take values 3.1, 3.9, and 3.2.

3.2. Phantom imaging

A set of gradient-echo images was acquired, changing WLC resonant frequency (i.e., adjusting the WLC tube length ℓ = 160–175 mm), while using the birdcage coil for transmission and reception. The blue curve in Fig. 4(c) shows the ratio of SNR in images acquired with and without the WLC present, as a function of ℓ, calculated in the breast phantom. A maximum SNR enhancement of 10.6 was achieved for ℓ = 172 mm, which corresponds to the resonant frequency of the WLC tuned to the Larmor frequency (f = 63.68 MHz). SNR maps for these cases are shown as insets in Fig. 4(c). We observe better than 5.9-fold SNR enhancement across the whole range of ℓ = 160–175 mm, suggesting that one can fix the length of tubes and use the WLC for different volunteers. To make a fair SNR comparison, the RF transmit voltage was adjusted for each measurement to produce the same flip angle within the ROI. At the maximum SNR gain, the transmit voltage was reduced by 87% of that required without the WLC present. Also, MR images captured with the WLC demonstrated the resolution improvement. The breast phantom structure is not ideally homogeneous; it contains several air bubbles formed as a result of the solidification of agarose. As shown in Supplementary Fig. 2 more detailed MR image was obtained using the WLC, and air bubbles (depicted by red circles) can be detected inside the phantom structure. Simultaneously, in the case of the birdcage coil used alone, the image is poor, and bubbles are impossible to distinguish.

4. Discussion and conclusion

The proposed idea of using a WLC as a transceiver for targeted breast imaging at 1.5 T has been carefully studied in this work, both numerically and experimentally. The proposed coil is based on a system of inductively coupled SLRs forming a resonator. The fundamental eigenmode of this WLC has a field distribution very similar to a conventional solenoid. However, conventional solenoids with a large cavity and homogeneous magnetic field distribution (suitable for extremities or breast) at 1.5 T are challenging to construct because their self-resonance frequencies are below 63.68 MHz due to inter-loop parasitic capacitance. In principle, it is possible to create a solenoid coil for clinical field strength (i.e., 1.5–3 T) with distributed capacitors. However, in this case, only several turns could be used that limits the coil's field-of-view and homogeneity of B_1-field. Meanwhile, the resonance frequency of metamaterial-inspired WLC can be tuned higher since individual loops are not connected electrically, and the overall number of loops could be increased to obtain a more homogeneous magnetic field distribution. When the resonant frequency of the fundamental eigenmode of the WLC is close to the resonant frequency of the body coil of the MRI system, inductive coupling between the coils causes the RF magnetic field to become focused inside the cavity of the WLC. Also, the WLC generates a fairly uniform magnetic field even though it is positioned off-center relative to the body coil. Thus the proposed WLC improves efficiency during transmission, reducing SAR, and improves sensitivity during reception increasing the SNR of acquired images.

As demonstrated numerically and by experimental studies with a phantom, the WLC increases SNR by factors of 6.4 and 10.6, respectively. This difference could be explained by different optimal coupling between the birdcage coil and WLC in simulation and experiment could be related to different positioning and load conditions of the birdcage coil and WLC, e.g., we have used slightly different body phantoms. In the meanwhile, the input voltage amplitude was substantially reduced improving the MR image resolution (see Supplementary Fig. 2).

Electromagnetic simulations using voxel models with different sizes showed the possibility of using WLC for females with different body mass indexes. In this case, the performance of the WLC vary in a small range: transmit efficiency gain changes in 4.2–5.8 times and SAR efficiency gain - 3.1–3.9 times. This fact is due to a decrease in the quality factor of the body coil and WLC associated with an increase in the load, which leads to a reduction of the amplitude of the RF magnetic field focused by the WLC. At the same time, the local maximum of $SAR_{av.\ 10\ g}$ for the same B_1^+ for the average load becomes 18 times lower in the presence of WLC than for a birdcage coil used alone. This is especially advantageous in cases where patients with metallic implants have to be scanned

or when high RF amplitude pulses are necessary to maintain optimal image quality.

In conclusion, we propose a WLC for targeted breast imaging, which is the first metamaterial inspired breast coil to boost the 1.5 T body coil's reception and transmission performances for relatively small regions of the body. Thus, we can potentially replace typical breast imaging setup. Instead of using a complicated and expensive local receive array, we can use an inductively coupled WLC. It is possible to use the WLC in combination with local receive array for other nuclei (e.g., sodium), or to adapt the design to combine different eigenmodes to make a heteronuclear WLC [23]. Since the proposed WLC supports linear polarization only (it interacts only with the H_y-component of the magnetic field), for a future study, it may be interesting to modify its design to operate in the CP mode regime. In the case of interaction with both H_x and H_y components, the WLC's efficiency will be enhanced by a factor of $\sqrt{2}$ [24]. Also, further study is needed to perform bilateral MRI with two WLC. We assume that the main difficulties here are mutual interaction between three resonators: two wireless coils and a birdcage coil, and loss in WLC's effectiveness. As was recently shown for the pair of dielectric resonators [25,26], a system of coupled resonant structures is characterized by two-hybrid eigenmodes (symmetric-like and anti-symmetric-like). So, it may be challenging to found the optimal tuning conditions for this system. Moreover, the usage of coupled modes of the pair of resonators leads to the $1/\sqrt{2}$ loss in SNR compared with single resonator imaging [26].

Nevertheless, the proposed idea of using a metamaterial inspired WLC can be directly integrated into an existing clinical system to make the procedure of MRI significantly safer for patients due to the lower level of SAR. Also, since WLC significantly boosts receive performance of the body coil, it can be considered as promising alternative to standard dedicated coils with a cable connection to the MR scanner, as was demonstrated in previous work for the wrist imaging [13].

Declaration of Competing Interest

The authors declare that they have no known competing financial interests or personal relationships that could have appeared to influence the work reported in this paper.

Acknowledgements

This work was supported by a grant from the Russian Science Foundation (No 18-75-10088). The authors express their gratitude to Dr. Alexander Efimtcev for assistance with MRI experiments and Dr. Anna Hurshkainen for useful discussions.

Appendix A. Supplementary material

Supplementary data associated with this article can be found, in the online version, at https://doi.org/10.1016/j.jmr.2020.106877.

References

[1] C.E. DeSantis, J. Ma, M.M. Gaudet, L.A. Newman, K.D. Miller, A.G. Sauer, A. Jemal, R.L. Siegel, Breast Cancer Statistics, 2019, CA Cancer J. Clin. 69 (6) (2019) 438–451, https://doi.org/10.3322/caac.21583.

[2] Z. Momenimovahed, H. Salehiniya, Epidemiological characteristics of and risk factors for breast cancer in the world, Breast Cancer - Targets and Therapy 11 (2019) 151–164, https://doi.org/10.2147/BCTT.S176070.

[3] V.P. Jackson, R.E. Hendrick, S.A. Feig, D.B. Kopans, Imaging of the radiographically dense breast, Radiology 188 (1993) 297–301, https://doi.org/10.1148/radiology.188.2.8327668.

[4] C.K. Kuhl, S. Schrading, C.C. Leutner, N. Morakkabati-Spitz, E. Wardelmann, R. Fimmers, W. Kuhn, H.H. Schild, Mammography, breast ultrasound, and magnetic resonance imaging for surveillance of women at high familial risk for breast cancer, J. Clin. Oncol. 23 (2005) 8469–8476, https://doi.org/10.1200/JCO.2004.00.4960.

[5] S. Juanpere, E. Perez, O. Huc, N. Motos, J. Pont, S. Pedraza, Imaging of breast implants-a pictorial review, Insights Imaging 2 (2011) 653–670, https://doi.org/10.1007/s13244-011-0122-3.

[6] G.L.G. Menezes, F.M. Knuttel, B.L. Stehouwer, R.M. Pijnappel, M.A. van den Bosch, Magnetic resonance imaging in breast cancer: A literature review and future perspectives, World J. Clin. Oncol. 5 (2) (2014) 61–70, https://doi.org/10.5306/wjco.v5.i2.61.

[7] C.K. Kuhl, S. Schrading, K. Strobel, H.H. Schild, R.D. Hilgers, H.B. Bieling, Abbreviated breast magnetic resonance imaging (MRI): first postcontrast subtracted images and maximum-intensity projection-a novel approach to breast cancer screening with MRI, J Clin Oncol. 32 (22) (2014) 2304–2310, https://doi.org/10.1200/JCO.2013.52.5386.

[8] A. Shchelokova, V. Ivanov, A. Mikhailovskaya, E. Kretov, I. Sushkov, S. Serebryakova, E. Nenasheva, I. Melchakova, P. Belov, A. Slobozhanyuk, A. Andreychenko, Ceramic resonators for targeted clinical magnetic resonance imaging of the breast, Nature Commun. 11 (2020) 3840, https://doi.org/10.1038/s41467-020-17598-3.

[9] M. Dietzel, E. Wenkel, M. Hammon, P. Clauser, M. Uder, R. Schulz-Wendtland, P.A.T. Baltzer, Does higher field strength translate into better diagnostic accuracy? A prospective comparison of breast MRI at 3 and 1.5 Tesla, Eur. J. Radiol. 114 (2019) 51–56, https://doi.org/10.1016/j.ejrad.2019.02.033.

[10] I. Zivkovic, W. Teeuwisse, A. Slobozhanyuk, E. Nenasheva, A. Webb, High permittivity ceramics improve the transmit field and receive efficiency of a commercial extremity coil at 1.5 Tesla, J. Magn. Reson. 299 (2019) 59–65, https://doi.org/10.1016/j.jmr.2018.12.013.

[11] A.V. Shchelokova, A.P. Slobozhanyuk, P. de Bruin, I. Zivkovic, E. Kallos, P.A. Belov, A. Webb, Experimental investigation of a metasurface resonator for in vivo imaging at 1.5 T, J. Magn. Reson. 286 (2018) 78–81, https://doi.org/10.1016/j.jmr.2017.11.013.

[12] A.V. Shchelokova, A.P. Slobozhanyuk, I.V. Melchakova, S.B. Glybovski, A.G. Webb, Y.S. Kivshar, P.A. Belov, Locally enhanced image quality with tunable hybrid metasurfaces, Phys. Rev. Appl. 9 (2018) 014020, https://doi.org/10.1103/PhysRevApplied.9.014020.

[13] A.V. Shchelokova, C.A.T. van den Berg, D.A. Dobrykh, S.B. Glybovski, M.A. Zubkov, E.A. Brui, D.S. Dmitriev, A.V. Kozachenko, A.Y. Efimtcev, A.V. Sokolov, V.A. Fokin, I.V. Melchakova, P.A. Belov, Volumetric wireless coil based on periodically coupled split-loop resonators for clinical wrist imaging, Magn. Reson. Med. 80 (4) (2018) 1726–1737, https://doi.org/10.1002/mrm.27140.

[14] S.I. Maslovski, P.M.T. Ikonen, I. Kolmakov, S.A. Tretyakov, M. Kaunisto, Artificial magnetic materials based on the new magnetic particle: metasolenoid, Progress In Electromagnetics Research 54 (2005) 61–81, https://doi.org/10.2528/PIER04101101.

[15] S. Itsukage, Y. Sowa, M. Goto, T. Taguchi, T. Numajiri, Breast volume measurement by recycling the data obtained from 2 routine modalities, mammography and magnetic resonance imaging, Eplasty 17 (2017) e39.

[16] L. Jylha, S. Maslovski, S. Tretyakov, High-order resonant modes of a metasolenoid, J. Electromagn. Waves Appl. 19 (10) (2005) 1327–1342, https://doi.org/10.1163/156939305775525891.

[17] A. V. Shchelokova, D. A. Dobrykh, S. B. Glybovski, I. V. Melchakova, P. A. Belov, A metasolenoid-like resonator for MRI applications, 2017 11th International Congress on Engineered Materials Platforms for Novel Wave Phenomena (Metamaterials), Marseille, 2017, pp. 82-84, doi: 10.1109/MetaMaterials.2017.8107846.

[18] A. Christ, W. Kainz, E.G. Hahn, K. Honegger, M. Zefferer, E. Neufeld, W. Rascher, R. Janka, W. Bautz, J. Chen, B. Kiefer, P. Schmitt, H.P. Hollenbach, J. Shen, M. Oberle, D. Szczerba, A. Kam, J.W. Guag, N. Kuster, The Virtual Family - development of surface-based anatomical models of two adults and two children for dosimetric simulations, Phys. Med. Biol. 55 (2) (2010) N23–38, https://doi.org/10.1088/0031-9155/55/2/N01.

[19] J.V. Rispoli, S.M. Wright, C.R. Malloy, M.P. McDougall, Automated modification and fusion of voxel models to construct body phantoms with heterogeneous breast tissue: Application to MRI simulations, J. Biomed. Graph Comput. 7 (1) (2017) 1–7, https://doi.org/10.5430/jbgc.v7n1p1.

[21] M.J. Burfeindt, T.J. Colgan, R.O. Mays, J.D. Shea, N. Behdad, B.D. Van Veen, S.C. Hagness, MRI-derived 3D-printed breast phantom for microwave breast imaging validation, IEEE Antennas Wirel. Propag. Lett. 11 (2012) 1610–1613, https://doi.org/10.1109/LAWP.2012.2236293.

[23] G. Solomakha, A. Hurshkainen, S. Glybovski, A. Andreychenko, Volume metasolenoid-based coil for ^{23}Na MRI at 7 Tesla, IOP Conf. Series: J. Phys.: Conf. Series 1461 (2020) 012056, https://doi.org/10.1088/1742-6596/1461/1/012056.

[24] G.H. Glover, C.E. Hayes, N.J. Pelc, W.A. Edelstein, O.M. Mueller, H.R. Hart, C.J. Hardy, M. O'Donnell, W.D. Barber, Comparison of linear and circular polarization for magnetic resonance imaging, J. Magn. Reson. 64 (2) (1969) 255–270, https://doi.org/10.1016/0022-2364(85)90349-X.

[25] V. Ivanov, A. Shchelokova, A. Andreychenko, A. Slobozhanyuk, Coupled very-high permittivity dielectric resonators for clinical MRI, Appl. Phys. Lett. 117 (10) (2020) 103701, https://doi.org/10.1063/5.0016086.

[26] M.A.C. Moussu, S.B. Glybovski, R. Abdeddaim, C. Craeye, S. Enoch, D. Tihon, S. Kurdjumov, M. Dubois, E. Georget, A.G. Webb, P. Belov, L. Ciobanu, Imaging of two samples with a single transmit/receive channel using coupled ceramic resonators for MR microscopy at 17.2 T, NMR Biomed. 33 (11) (2020) e4397, https://doi.org/10.1002/nbm.4397.